

Improvement in Fast Particle Track Reconstruction with Robust Statistics

M. G. Aartsen², R. Abbasi²⁷, Y. Abdou²², M. Ackermann⁴², J. Adams¹⁵,
J. A. Aguilar²¹, M. Ahlers²⁷, D. Altmann⁹, J. Auffenberg²⁷, X. Bai^{31,1},
M. Baker²⁷, S. W. Barwick²³, V. Baum²⁸, R. Bay⁷, J. J. Beatty^{17,18},
S. Bechet¹², J. Becker Tjus¹⁰, K.-H. Becker⁴¹, M. L. Benabderrahmane⁴²,
S. BenZvi²⁷, P. Berghaus⁴², D. Berley¹⁶, E. Bernardini⁴², A. Bernhard³⁰,
D. Z. Besson²⁵, G. Binder^{8,7}, D. Bindig⁴¹, M. Bissok¹, E. Blaufuss¹⁶,
J. Blumenthal¹, D. J. Boersma⁴⁰, S. Bohachuk²⁰, C. Boehm³⁴, D. Bose¹³,
S. Böser¹¹, O. Botner⁴⁰, L. Brayeur¹³, H.-P. Bretz⁴², A. M. Brown¹⁵,
R. Bruijn²⁴, J. Brunner⁴², M. Carson²², J. Casey⁵, M. Casier¹³, D. Chirkin²⁷,
A. Christov²¹, B. Christy¹⁶, K. Clark³⁹, F. Clevermann¹⁹, S. Coenders¹,
S. Cohen²⁴, D. F. Cowen^{39,38}, A. H. Cruz Silva⁴², M. Danninger³⁴,
J. Daughhetee⁵, J. C. Davis¹⁷, M. Day²⁷, C. De Clercq¹³, S. De Ridder²²,
P. Desiati²⁷, K. D. de Vries¹³, M. de With⁹, T. DeYoung³⁹, J. C. Díaz-Vélez²⁷,
M. Dunkman³⁹, R. Eagan³⁹, B. Eberhardt²⁸, J. Eisch²⁷, S. Euler¹,
P. A. Evenson³¹, O. Fadiran²⁷, A. R. Fazely⁶, A. Fedynitch¹⁰, J. Feintzeig²⁷,
T. Feusels²², K. Filimonov⁷, C. Finley³⁴, T. Fischer-Wasels⁴¹, S. Flis³⁴,
A. Franckowiak¹¹, K. Frantzen¹⁹, T. Fuchs¹⁹, T. K. Gaisser³¹, J. Gallagher²⁶,
L. Gerhardt^{8,7}, L. Gladstone²⁷, T. Glüsenskamp⁴², A. Goldschmidt⁸,
G. Golup¹³, J. G. Gonzalez³¹, J. A. Goodman¹⁶, D. Góra⁴²,
D. T. Grandmont²⁰, D. Grant²⁰, A. Groß³⁰, C. Ha^{8,7}, A. Haj Ismail²²,
P. Hallen¹, A. Hallgren⁴⁰, F. Halzen²⁷, K. Hanson¹², D. Heereman¹²,
D. Heinen¹, K. Helbing⁴¹, R. Hellauer¹⁶, S. Hickford¹⁵, G. C. Hill²,
K. D. Hoffman¹⁶, R. Hoffmann⁴¹, A. Homeier¹¹, K. Hoshina²⁷,
W. Huelsnitz^{16,2}, P. O. Hulth³⁴, K. Hultqvist³⁴, S. Hussain³¹, A. Ishihara¹⁴,
E. Jacobi⁴², J. Jacobsen²⁷, K. Jagielski¹, G. S. Japaridze⁴, K. Jero²⁷,
O. Jlelati²², B. Kaminsky⁴², A. Kappes⁹, T. Karg⁴², A. Karle²⁷, J. L. Kelley²⁷,
J. Kiryluk³⁵, J. Kläs⁴¹, S. R. Klein^{8,7}, J.-H. Köhne¹⁹, G. Kohnen²⁹,
H. Kolanoski⁹, L. Köpke²⁸, C. Kopper²⁷, S. Kopper⁴¹, D. J. Koskinen³⁹,
M. Kowalski¹¹, M. Krasberg²⁷, K. Krings¹, G. Kroll²⁸, J. Kunnen¹³,
N. Kurahashi²⁷, T. Kuwabara³¹, M. Labare²², H. Landsman²⁷, M. J. Larson³⁷,
M. Lesiak-Bzdak³⁵, M. Leuermann¹, J. Leute³⁰, J. Lünemann²⁸, O. Macías¹⁵,
J. Madsen³³, G. Maggi¹³, R. Maruyama²⁷, K. Mase¹⁴, H. S. Matis⁸,
F. McNally²⁷, K. Meagher¹⁶, M. Merck²⁷, T. Meures¹², S. Miarecki^{8,7},
E. Middell⁴², N. Milke¹⁹, J. Miller¹³, L. Mohrmann⁴², T. Montaruli^{21,3},

*Corresponding author. Email: wellons@icecube.wisc.edu, Phone: 304-542-4464, Address: Wisconsin Institutes for Discovery, 330 N. Orchard St., Madison, WI 53715

¹Physics Department, South Dakota School of Mines and Technology, Rapid City, SD 57701, USA

²Los Alamos National Laboratory, Los Alamos, NM 87545, USA

³also Sezione INFN, Dipartimento di Fisica, I-70126, Bari, Italy

⁴NASA Goddard Space Flight Center, Greenbelt, MD 20771, USA

37 R. Morse²⁷, R. Nahnauer⁴², U. Naumann⁴¹, H. Niederhausen³⁵,
 38 S. C. Nowicki²⁰, D. R. Nygren⁸, A. Obertacke⁴¹, S. Odrowski²⁰, A. Olivas¹⁶,
 39 A. Omairat⁴¹, A. O'Murchadha¹², L. Paul¹, J. A. Pepper³⁷,
 40 C. Pérez de los Heros⁴⁰, C. Pfendner¹⁷, D. Pieloth¹⁹, E. Pinat¹², J. Posselt⁴¹,
 41 P. B. Price⁷, G. T. Przybylski⁸, L. Rädcl¹, M. Rameez²¹, K. Rawlins³,
 42 P. Redl¹⁶, R. Reimann¹, E. Resconi³⁰, W. Rhode¹⁹, M. Ribordy²⁴,
 43 M. Richman¹⁶, B. Riedel²⁷, J. P. Rodrigues²⁷, C. Rott³⁶, T. Ruhe¹⁹,
 44 B. Ruzybayev³¹, D. Ryckbosch²², S. M. Saba¹⁰, T. Salameh³⁹, H.-G. Sander²⁸,
 45 M. Santander²⁷, S. Sarkar³², K. Schatto²⁸, F. Scheriau¹⁹, T. Schmidt¹⁶,
 46 M. Schmitz¹⁹, S. Schoenen¹, S. Schöneberg¹⁰, A. Schönwald⁴², A. Schukraft¹,
 47 L. Schulte¹¹, O. Schulz³⁰, D. Seckel³¹, Y. Sestayo³⁰, S. Seunarine³³,
 48 R. Shanidze⁴², C. Sheremata²⁰, M. W. E. Smith³⁹, D. Soldin⁴¹,
 49 G. M. Spiczak³³, C. Spiering⁴², M. Stamatikos^{17,4}, T. Stanev³¹, A. Stasik¹¹,
 50 T. Stezelberger⁸, R. G. Stokstad⁸, A. Stöbl⁴², E. A. Strahler¹³, R. Ström⁴⁰,
 51 G. W. Sullivan¹⁶, H. Taavola⁴⁰, I. Taboada⁵, A. Tamburro³¹, A. Tepe⁴¹,
 52 S. Ter-Antonyan⁶, G. Tešić³⁹, S. Tilav³¹, P. A. Toale³⁷, S. Toscano²⁷,
 53 E. Unger¹⁰, M. Usner¹¹, S. Vallecorsa²¹, N. van Eijndhoven¹³,
 54 A. Van Overloop²², J. van Santen²⁷, M. Vehring¹, M. Voge¹¹, M. Vraeghe²²,
 55 C. Walck³⁴, T. Waldenmaier⁹, M. Wallraff¹, Ch. Weaver²⁷, M. Wellons²⁷,
 56 C. Wendt²⁷, S. Westerhoff²⁷, N. Whitehorn²⁷, K. Wiebe²⁸, C. H. Wiebusch¹,
 57 D. R. Williams³⁷, H. Wissing¹⁶, M. Wolf³⁴, T. R. Wood²⁰, K. Woschnagg⁷,
 58 D. L. Xu³⁷, X. W. Xu⁶, J. P. Yanez⁴², G. Yodh²³, S. Yoshida¹⁴,
 59 P. Zarzhitsky³⁷, J. Ziemann¹⁹, S. Zierke¹, M. Zoll³⁴, B. Recht⁴³, C. Ré⁴³

60 ¹*III. Physikalisches Institut, RWTH Aachen University, D-52056 Aachen, Germany*

61 ²*School of Chemistry & Physics, University of Adelaide, Adelaide SA, 5005 Australia*

62 ³*Dept. of Physics and Astronomy, University of Alaska Anchorage, 3211 Providence Dr.,*
 63 *Anchorage, AK 99508, USA*

64 ⁴*CTSPS, Clark-Atlanta University, Atlanta, GA 30314, USA*

65 ⁵*School of Physics and Center for Relativistic Astrophysics, Georgia Institute of*
 66 *Technology, Atlanta, GA 30332, USA*

67 ⁶*Dept. of Physics, Southern University, Baton Rouge, LA 70813, USA*

68 ⁷*Dept. of Physics, University of California, Berkeley, CA 94720, USA*

69 ⁸*Lawrence Berkeley National Laboratory, Berkeley, CA 94720, USA*

70 ⁹*Institut für Physik, Humboldt-Universität zu Berlin, D-12489 Berlin, Germany*

71 ¹⁰*Fakultät für Physik & Astronomie, Ruhr-Universität Bochum, D-44780 Bochum,*
 72 *Germany*

73 ¹¹*Physikalisches Institut, Universität Bonn, Nussallee 12, D-53115 Bonn, Germany*

74 ¹²*Université Libre de Bruxelles, Science Faculty CP230, B-1050 Brussels, Belgium*

75 ¹³*Vrije Universiteit Brussel, Dienst ELEM, B-1050 Brussels, Belgium*

76 ¹⁴*Dept. of Physics, Chiba University, Chiba 263-8522, Japan*

77 ¹⁵*Dept. of Physics and Astronomy, University of Canterbury, Private Bag 4800,*
 78 *Christchurch, New Zealand*

79 ¹⁶*Dept. of Physics, University of Maryland, College Park, MD 20742, USA*

80 ¹⁷*Dept. of Physics and Center for Cosmology and Astro-Particle Physics, Ohio State*
 81 *University, Columbus, OH 43210, USA*

82 ¹⁸*Dept. of Astronomy, Ohio State University, Columbus, OH 43210, USA*

83 ¹⁹*Dept. of Physics, TU Dortmund University, D-44221 Dortmund, Germany*

84 ²⁰*Dept. of Physics, University of Alberta, Edmonton, Alberta, Canada T6G 2E1*

85 ²¹*Département de physique nucléaire et corpusculaire, Université de Genève, CH-1211*
 86 *Genève, Switzerland*

87 ²²*Dept. of Physics and Astronomy, University of Gent, B-9000 Gent, Belgium*

- 88 ²³Dept. of Physics and Astronomy, University of California, Irvine, CA 92697, USA
89 ²⁴Laboratory for High Energy Physics, École Polytechnique Fédérale, CH-1015 Lausanne,
90 Switzerland
91 ²⁵Dept. of Physics and Astronomy, University of Kansas, Lawrence, KS 66045, USA
92 ²⁶Dept. of Astronomy, University of Wisconsin, Madison, WI 53706, USA
93 ²⁷Dept. of Physics and Wisconsin IceCube Particle Astrophysics Center, University of
94 Wisconsin, Madison, WI 53706, USA
95 ²⁸Institute of Physics, University of Mainz, Staudinger Weg 7, D-55099 Mainz, Germany
96 ²⁹Université de Mons, 7000 Mons, Belgium
97 ³⁰T.U. Munich, D-85748 Garching, Germany
98 ³¹Bartol Research Institute and Department of Physics and Astronomy, University of
99 Delaware, Newark, DE 19716, USA
100 ³²Dept. of Physics, University of Oxford, 1 Keble Road, Oxford OX1 3NP, UK
101 ³³Dept. of Physics, University of Wisconsin, River Falls, WI 54022, USA
102 ³⁴Oskar Klein Centre and Dept. of Physics, Stockholm University, SE-10691 Stockholm,
103 Sweden
104 ³⁵Department of Physics and Astronomy, Stony Brook University, Stony Brook, NY
105 11794-3800, USA
106 ³⁶Department of Physics, Sungkyunkwan University, Suwon 440-746, Korea
107 ³⁷Dept. of Physics and Astronomy, University of Alabama, Tuscaloosa, AL 35487, USA
108 ³⁸Dept. of Astronomy and Astrophysics, Pennsylvania State University, University Park,
109 PA 16802, USA
110 ³⁹Dept. of Physics, Pennsylvania State University, University Park, PA 16802, USA
111 ⁴⁰Dept. of Physics and Astronomy, Uppsala University, Box 516, S-75120 Uppsala, Sweden
112 ⁴¹Dept. of Physics, University of Wuppertal, D-42119 Wuppertal, Germany
113 ⁴²DESY, D-15735 Zeuthen, Germany
114 ⁴³Dept. of Computer Sciences, University of Wisconsin, Madison, WI 53706, USA

115 **Abstract**

116 The IceCube project has transformed one cubic kilometer of deep natural
117 Antarctic ice into a Cherenkov detector. Muon neutrinos are detected and their
118 direction inferred by mapping the light produced by the secondary muon track
119 inside the volume instrumented with photomultipliers. Reconstructing of the
120 muon track from the observed light is challenging due to noise, light scattering
121 in the ice medium, and the possibility of simultaneously having multiple muons
122 inside the detector resulting from the large flux of cosmic ray muons.

123 This manuscript describes work on two problems: (1) the *track reconstruction*
124 *problem*, in which, given a set of observations, the goal is to recover the
125 track of a muon, and (2) the *coincident event problem*, which is to determine
126 how many muons are active in the detector during a time window. Rather than
127 solving these problems by developing more complex physical models that are
128 applied at later stages of the analysis, our approach is to augment the detector's
129 early reconstruction with data filters and robust statistical techniques. These
130 can be implemented at the level of on-line reconstruction and therefore improve
131 all subsequent reconstructions. Using the metric of median angular resolution, a
132 standard metric for track reconstruction, we improve the accuracy in the initial
133 reconstruction direction by 13%. We also present improvements in measuring
134 the number of muons in coincident events: we can accurately determine the

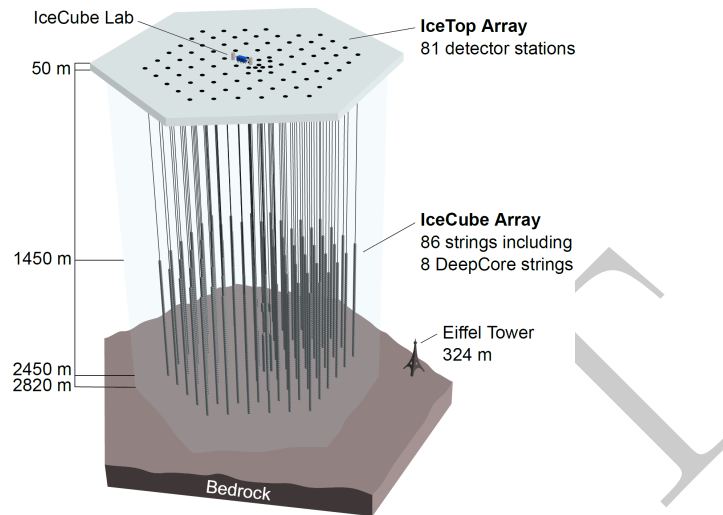


Figure 1: The IceCube neutrino detector in the Antarctic ice. A picture of the Eiffel Tower is shown for scale.

135 number of muons 98% of the time, which is an improvement of 86% over the
 136 software previously used in IceCube.

137 *Keywords:* IceCube, Track reconstruction, Neutrino telescope, Neutrino
 138 astrophysics, Robust Statistics

139 **1. Introduction**

140 The IceCube neutrino detector searches for neutrinos that are generated by
 141 the universe’s most violent astrophysical events: exploding stars, gamma ray
 142 bursts, and cataclysmic phenomena involving black holes and neutron stars [1].
 143 The detector, roughly one cubic kilometer in size, is located near the geographic
 144 South Pole and is buried to a depth of about 2.5 km in the Antarctic ice [2].
 145 The detector is illustrated in Figure 1 and a more complete description is given
 146 in Section 2.

147 When a neutrino enters the telescope, it occasionally interacts in the ice and
 148 generates a muon. The neutrino direction can be inferred from a reconstruction
 149 of the muon track. Muons are also generated by cosmic rays interacting
 150 in the atmosphere, and separation of the background of cosmic ray muons and
 151 neutrino-induced muons is a necessary step for neutrino analysis. This separation
 152 is challenging, as the number of observed cosmic ray muons exceeds the
 153 number of observed neutrino muons by over five orders of magnitude [3].

154 The primary mechanism for separating the cosmic ray muons from the neu-
 155 trino muons is reconstructing the muon track and determining whether the

156 muon was traveling downwards into the Earth or upwards out of the Earth.
157 Since neutrinos can penetrate through the Earth but cosmic ray muons cannot,
158 it follows that a muon traveling out of the Earth must have been generated by a
159 neutrino. Thus, by selecting only the muons that are reconstructed as up-going,
160 the cosmic ray muons can, in principle, be removed from the data. Since the
161 number of cosmic ray muons overwhelms the number of neutrino muons, high
162 accuracy is critical for preventing erroneous reconstruction of cosmic ray muons
163 as neutrino-induced.

164 Here, we examine two problems that arise in the separation of cosmic ray
165 muons from neutrino muons in the IceCube detector:

- 166 1. *Reconstruction*, in which the track of a muon is reconstructed from the
167 observed light at different positions and times in the detector.
- 168 2. *Coincident Event Detection*, in which we detect the number of muons
169 inside the detector, and assign observed photons to a muon.

170 Sophisticated reconstruction techniques have been developed that computa-
171 tionally model in detail the muon’s Cherenkov cone as well as the scattering
172 and absorption of photons through layers of Antarctic ice with varying optical
173 properties [3–5]. Rather than further refining these techniques, the current work
174 focusses on improving the statistical techniques and optimizing data filtering in
175 the early online track reconstruction performed on the data in real time at the
176 South Pole. Besides benefiting directly any analysis that uses the online recon-
177 struction such as the search for cosmogenic neutrinos, any later analysis will
178 benefit from improvements made at the early stages of the data collection.

179 1.1. *Related Work*

180 Track reconstruction and coincident event detection challenges are ubiqui-
181 tous in particle physics [6–8], both in particle accelerators and cosmic particle
182 detectors. While the work described in this manuscript builds on the previous
183 technique developed for the IceCube detector [3], these techniques are general
184 purpose, and potentially have applications in detectors beyond IceCube.

185 1.2. *Outline*

186 We begin by describing the IceCube detector and track reconstruction chal-
187 lenges in Section 2. In Section 3, we describe the reconstruction pipeline in-
188 cluding the prior IceCube software, then we present improvements to the online
189 tracking algorithm and discuss the results. Section 4 describes improvements
190 on coincident event detection, and follows a parallel structure to Section 3. We
191 conclude in Section 5.

192 2. IceCube Detector and Track Reconstruction Challenges

193 The IceCube detector is composed of 5,160 optical detectors, each containing
194 a photomultiplier tube (PMT) and onboard digitizer [9]. The PMTs are spread
195 over 86 vertical strings arranged in a hexagonal shape, with a total instrumented

196 volume of approximately one cubic kilometer. The PMTs on a given string
197 are separated vertically by 17 m, and the string-to-string separation is roughly
198 125 m.

199 At an abstract level, the IceCube detector operates by detecting muons
200 as they travel through the instrumented volume of ice. As the muon travels
201 through the detector, it radiates light [4], which is observed by the PMTs and
202 quantized into discrete *hits* [10]. The detector uses several trigger criteria. The
203 most commonly used trigger selects time intervals where eight PMTs (with local
204 coincidences) fired within 5 microseconds. When a trigger occurs, all data within
205 a 10 microsecond trigger window is saved, becoming an *event*. If the number of
206 hits in an event is sufficiently large, the muon track reconstruction algorithm is
207 triggered.

208 There are several challenges for the reconstruction algorithms used in the
209 detector. Varying optical properties of the ice affect reconstruction accuracy,
210 the data may contain outlier hits due to uncorrelated noise, and there are finite
211 computational resources available to tracking code run on-site.

212 *Modeling Difficulties.* The details of the ice’s optical properties are nontrivial to
213 model. Light propagating through the ice is affected by scattering and absorp-
214 tion. These effects cannot be analytically calculated and the optical properties
215 of the ice vary with depth [5]. In addition, the Cherenkov light originates both
216 directly from the muon, and from particles showers initiated by stochastic en-
217 ergy losses of the muon.

218 *Noise.* The noise inherent in the data is another challenge. Noise hits can
219 arise either from the thermal background of the photocathode, or from photons
220 generated by radioactive decay inside the PMT [9].

221 *Computational Constraints.* The reconstruction algorithms are also limited in
222 complexity by the computing resources available at the South Pole. The track
223 reconstruction algorithm has to process about 3,000 muons per second, algo-
224 rithms with excessive computational demands are discouraged.

225 **3. Reconstruction Improvement**

226 As shown in the following, augmenting the reconstruction algorithm with
227 some basic filters and classical data analysis techniques results in significant
228 improvement in the reconstruction algorithm’s accuracy.

229 *3.1. Prior IceCube Software*

230 The muon track reconstruction process (outlined in Figure 2) starts when the
231 number of detected hits exceeds a preset threshold and initiates data collection.
232 After the initial data are collected, the event then passes through a series of
233 basic filters to remove obvious outliers [11].

234 This is followed by a basic reconstruction algorithm, *linefit* [12], that disre-
235 gards the Cherenkov cone and instead finds the track that minimizes the sum

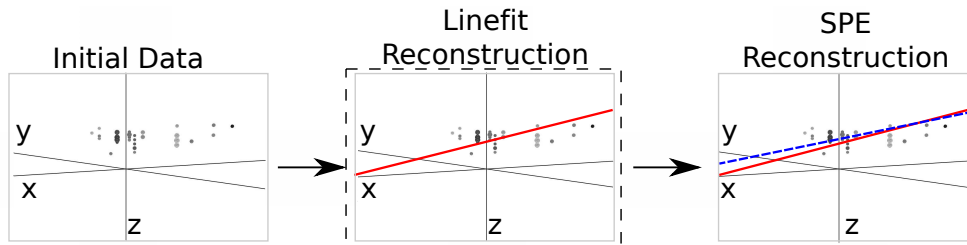


Figure 2: The reconstruction pipeline used to process data in the IceCube detector. After initial data are collected, it is then processed by some basic noise filters, which remove clear outliers. This cleaned data are processed by a basic reconstruction algorithm (solid line), which is used as the seed for the more sophisticated reconstruction algorithm (dashed line). The sophisticated reconstruction is then evaluated as a potential neutrino. The work presented in this manuscript makes changes to the basic reconstruction step (indicated by the dashed box).

236 of the squares of the distances between the track and the hits. More formally,
 237 assume there are N hits; denote the position and time of the i th hit as \vec{x}_i and t_i ,
 238 respectively. Let the reconstructed muon track have a velocity of \vec{v} , and let the
 239 reconstructed track pass through point \vec{x}_0 at time t_0 . Then linefit reconstruction
 240 solves the *least-squares* optimization problem

$$\min_{t_0, \vec{x}_0, \vec{v}} \sum_{i=1}^N \rho_i(t_0, \vec{x}_0, \vec{v})^2, \quad (1)$$

241 where

$$\rho_i(t_0, \vec{x}_0, \vec{v}) = \|\vec{v}(t_i - t_0) + \vec{x}_0 - \vec{x}_i\|_2. \quad (2)$$

242 Linefit is an approximation primarily used to generate an initial track or *seed*
 243 for a more sophisticated reconstruction.

244 The reconstruction algorithm for the sophisticated reconstruction is *Single-*
 245 *Photo-Electron-Fit (SPE fit)* [3]. SPE fit uses the least-squares reconstruction,
 246 the event data, and a parameterized probability distribution function of scatter-
 247 ing in ice [3] to reconstruct the muon track. The SPE fit is the primary
 248 reconstruction algorithm used in the initial data selection and filtering run at
 249 the detector site, and the fit serves as a seed track to the more complex recon-
 250 structions used in off-site data analyses.

251 3.2. Algorithm Improvement

252 If angular deviations of the initial seed are large (>5 -10 degrees), the simple
 253 subsequent reconstruction, SPE, often does not converge to the global minimum
 254 and the efficiency is degraded. This can be resolved by more advanced but
 255 time consuming reconstruction algorithms or by improving the initial seed as
 256 described here.

257 As indicated in Equation 1, a least-squares fit models the muon as a single
 258 point moving in a straight line, and hits are penalized quadratically in their

259 distance from this line. Thus there is an implicit assumption in this model:
 260 that all the hits will be near the muon. This assumption has several pitfalls:

- 261 1. It doesn't account for the distinct Cherenkov emission profile from the
 262 muon.
- 263 2. It ignores the scattering effects of the ice medium. Some of the photons can
 264 scatter for over a microsecond, which means that when they are recorded
 265 by a PMT, the muon will be over 300 m away.
- 266 3. While the noise reduction steps remove most of the outlier noise, the noise
 267 hits that survive can be far from the muon. Since these outliers are given
 268 quadratic weight, they exert a huge influence over the model.

269 The first two pitfall occur because the model is incomplete and does not
 270 accurately model the data, and the third demonstrates that the model is not
 271 robust to noise. The solution to this is twofold: improve the model and increase
 272 the noise robustness by replacing least squares with robust statistical techniques.

273 3.2.1. Improving the Model

274 While disregarding the Cherenkov profile is inherent to the simplified model
 275 chosen for speed reasons, removing hits generated by photons that scattered
 276 for a significant length of time will mitigate the effect of ignoring the photon
 277 scattering in the ice. We found that a basic filter could identify these scattered
 278 hits, and improve accuracy by almost a factor of two by removing them from
 279 the dataset.

280 More formally, for each hit h_i , the algorithm looks at all neighboring hits
 281 within a neighborhood of r , and if there exists a neighboring hit h_j with a time
 282 stamp that is t earlier than h_i , then h_i is considered a scattered hit, and is
 283 not used in the basic reconstruction algorithm. Optimal values of r and t were
 284 found to be 156 m and 778 ns by tuning them on simulated muon data with an
 285 E^{-2} power law spectrum.

286 3.2.2. Adding Robustness to Noise

287 As described in equation 1, the least squares model gives outliers quadratic
 288 weight, whereas we would prefer that outliers had zero weight. There are robust
 289 models in classical statistics designed to marginalize outliers. We determined
 290 that replacing the least-squares model with a Huber fit [13] improves the recon-
 291 struction accuracy.

292 More formally, we replace Equation 1 with the optimization problem:

$$\min_{t_0, \vec{x}_0, \vec{v}} \sum_{i=1}^N \phi(\rho_i(t_0, \vec{x}_0, \vec{v})), \quad (3)$$

293 where the Huber penalty function $\phi(\rho)$ is defined as

$$\phi(\rho) \equiv \begin{cases} \rho^2 & \text{if } \rho < \mu \\ \mu(2\rho - \mu) & \text{if } \rho \geq \mu \end{cases} . \quad (4)$$

Table 1: Median angular resolution (degrees) for reconstruction improvements. The first line is the accuracy of the prior least-squares model, and the subsequent lines are the accuracy measurements from cumulatively adding improvements into the basic reconstruction algorithm.

Algorithm	θ_{med}
Linefit Reconstruction (Least-Squares)	9.917
With Addition of Logical Filter	5.205
With Addition of Huber Regression	4.672
With Addition of Outlier Removal	4.211

294 Here, $\rho_i(t_0, \vec{x}, \vec{v})$ is defined in Equation 2 and μ is a constant calibrated to the
 295 data (on simulated muon events with an E^{-2} power law spectrum, the optimal
 296 value of μ is 153 m).

297 The Huber penalty function has two regimes. In the near-hit regime ($\rho < \mu$),
 298 hits are assumed to be strongly correlated with the muon’s track, and the Huber
 299 penalty function behaves like least squares, giving these hits quadratic weight.
 300 In the far-hit regime ($\rho \geq \mu$), hits are given linear weights as they are more
 301 likely to be noise.

302 In addition to its attractive robustness properties, the Huber fit’s weight
 303 assignment also has the added benefit that it inherently labels points as outliers
 304 (those with $\rho \geq \mu$). Thus, once the Huber fit is computed, we can go one step
 305 farther and simply remove the labeled outliers from the dataset. A better fit is
 306 then obtained by computing the least-squares fit on the data with the outliers
 307 removed. The entire algorithm has a mean runtime that is approximately six
 308 times longer than Linefit’s mean runtime.

309 3.3. Results

310 The goal is to improve the accuracy of the reconstruction in order to better
 311 separate neutrinos from cosmic rays. Thus we present three measurements: (1)
 312 the accuracy change between linefit and the new algorithm, (2) the accuracy
 313 change when SPE is seeded with the new algorithm instead of linefit, and (3)
 314 the improvement in separation between neutrinos and cosmic rays.

315 To measure the improvement generated by the changes, we use the metric
 316 of *median angular resolution* θ_{med} . The angular resolution of a reconstruction
 317 is the arc-distance between the reconstruction and the true track. The dataset
 318 is drawn from simulated neutrino data designed to be similar to that observed
 319 by the detector.

320 We can improve the median angular resolution of the basic reconstruction
 321 by 57.6%, as shown in Table 1. Seeding SPE with the improved basic recon-
 322 struction generates an improvement in the angular resolution of 12.9%. These
 323 improvements in the reconstruction algorithm result in 10% fewer atmospheric
 324 muons erroneously reconstructed as up-going, and 1% more muons correctly
 325 reconstructed as up-going.

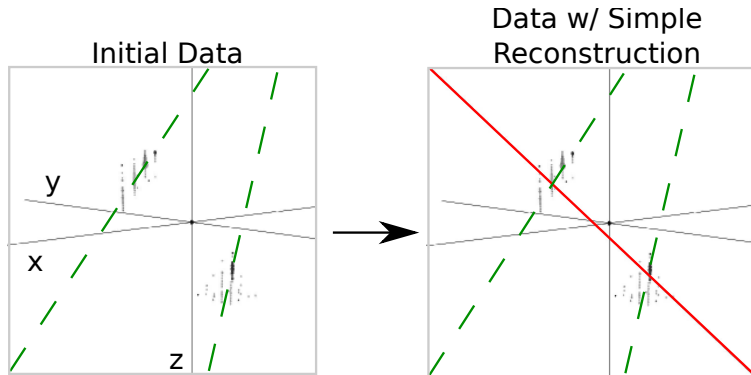


Figure 3: In this example, an event that is clearly composed of two muons (actual tracks shown as dashed lines) is treated as a single muon, and thus the reconstruction (solid line) is inaccurate.

326 4. Coincident Event Improvements

327 In the second study, we look at the problem of determining when more than
 328 one muon has entered the detector. In the most common case, a single muon
 329 will pass through the detector and generate an event before exiting. These events
 330 are processed by the pipeline described in Figure 2. However, for roughly 9%
 331 of the events collected by the data collection algorithm, more than one muon
 332 will be passing through the detector simultaneously, an occurrence known as a
 333 *coincident event*.

334 One of the primary sources of background noise in IceCube analyses is coinci-
 335 dent background muons that have been erroneously reconstructed as neutrinos.
 336 To see why this occurs, consider the coincident event shown in Figure 3. There
 337 are two clear groups of hits; however, the reconstruction algorithm treats them
 338 as a single group, resulting in an erroneous reconstruction. In the ideal case,
 339 the reconstruction algorithm would identify coincident events and split them,
 340 as in Figure 4.

341 The challenge in this example is determining the number of muons in an
 342 event. Our studies show that a simple spatial clustering algorithm can solve
 343 this classification problem with less than 2% error.

344 4.1. Prior IceCube Software

345 Coincident events have been a concern in the IceCube analysis [14] for years,
 346 and some software has been developed to handle coincident events. As a baseline
 347 of comparison, we use the *TTrigger* software, which is described in [15].

348 4.2. Algorithm Improvement

349 Here we present a proximal clustering algorithm. The intuition in proximal
 350 clustering is that points local in space and time are probably from the same

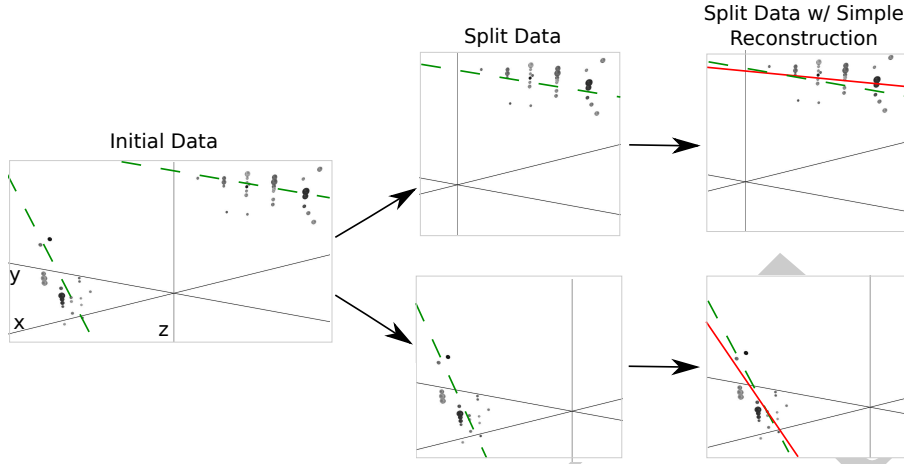


Figure 4: Ideally, the detector would split coincident events before computing the reconstruction. Splitting the event results in more accurate reconstructions (reconstructions shown as solid lines, true muon tracks shown as dashed lines). Note the difference in the reconstructions compared with Figure 3.

351 muon. The proximal clustering algorithm iterates through each pair of hits
 352 (i, j) and builds an adjacency matrix \mathbf{A} as

$$\mathbf{A}_{ij} = \begin{cases} 1 & \text{if } \|\Delta x^2 + \Delta y^2 + \Delta z^2 + (c\Delta t)^2\|_2 \leq \alpha, \\ 0 & \text{otherwise} \end{cases} \quad (5)$$

353 where $\Delta x, \Delta y, \Delta z$ and Δt are the space and time differences between the pair
 354 of hits, and α is tuned to the data (in this application, the optimal value of
 355 α is 450 m). The clustering can be recovered by extracting the connected
 356 components of the graph defined by \mathbf{A} . A connected component of a graph is a
 357 subgraph such that there exist a path between any two vertices of this subgraph.

358 4.2.1. Improving the Model

359 When implemented naively, proximal clustering succeeded for the majority
 360 of the events, but failed if there was a gap in the muon track, which can occur
 361 when the muon travels through dusty ice layers with short scattering length. If
 362 there is a significantly large gap, the algorithm erroneously separates the hits
 363 into two clusters.

364 To compensate, an additional heuristic is added, *track connecting*. After the
 365 data segmentation is finished, track connecting determines if separate clusters
 366 should be combined. It computes the mean position and time of each cluster,
 367 and connects a hypothetical muon track T between each pair of subspaces.

368 It checks if the speed s of the hypothetical track is within 25% of the speed
 369 of light c , and it checks that the mean distance between hits and T in both
 370 clusters is less than 60 m. If T passes both checks, the clusters are combined.

371 *4.2.2. Adding Robustness to Noise*

372 Proximal clustering is susceptible to noise. Noise hits close to two disjoint
373 tracks will be considered adjacent to both tracks, and thus can connect the two
374 tracks in the adjacency matrix.

375 One heuristic that worked well at mitigating this problem was to not use
376 all the hits in building the adjacency matrix. During data collection, some hits
377 are flagged as having a *local coincidence condition*, which indicates that both
378 they and a neighboring PMT reported a hit. These hits have a high probability
379 of not being noise hits, and thus exclusively using them to build the adjacency
380 matrix mitigates the problem of erroneously connecting two tracks.

381 After the proximal clustering algorithm has extracted the tracks from the
382 adjacency matrix, the hits not used in the construction of the adjacency matrix
383 are simply assigned to the closest reconstructed track.

384 *4.3. Results*

385 There were two competing goals for coincident event detection algorithms:
386 the algorithm should be conservative enough that events containing single tracks
387 are not erroneously split, and aggressive enough that a useful fraction of coin-
388 cident events are split correctly. Our algorithm is tuned to keep almost all
389 of the single events correctly unsplit, while still correctly splitting 80% of the
390 coincident events.

391 *4.3.1. Measurements*

392 We modified the reconstruction pipeline shown in Figure 2, in between the
393 noise cleaning and the basic reconstruction, by adding a step for coincident event
394 detection, as shown in Figure 4. This step takes cleaned data and attempts to
395 classify the event as a single-track or multiple-track event.

396 We ran each algorithm on two datasets of simulated data. One dataset
397 comprised single-muon events, and the other dataset comprised multiple-muon
398 events. In each dataset, we measured the classification error E , which is the
399 fraction of events that were misclassified. To get a global measurement, we
400 compute the *total error* E_{tot} , defined as

$$E_{tot} = w_{\text{Single}} E_{\text{Single}} + \alpha w_{\text{Multiple}} E_{\text{Multiple}}. \quad (6)$$

401 For computing E_{tot} , we use $w_{\text{Single}} = 0.917$ and $w_{\text{Multiple}} = 0.083$, which is
402 the frequency in which single-muon and multiple-muon events appear in data
403 simulating the distribution of events that trigger the reconstruction algorithm.
404 We also include a factor of α in the weighting of the multiple-muon events. This
405 factor expresses that mischaracterizing a multiple-muon event as a single-muon
406 event degrades the quality of most higher-order analysis more than the reverse
407 mischaracterization. In our calculations we use a value of $\alpha = 5$.

408 We present the results for the coincident event problem by measuring how
409 well each algorithm performs at determining the number of subspaces in an
410 event.

Table 2: Error Rates for Classification Algorithms

Algorithm	$E_{\text{Single}}\%$	$E_{\text{Multiple}}\%$	$E_{\text{tot}}\%$
Trivial	0.0	100.0	41.5
TTrigger	11.5	31.8	23.7
Proximal clustering	0.2	18.9	8.0

411 There are two natural comparisons for the work: the prior software TTrigger,
 412 as well as the trivial algorithm, which always classifies each event as a single-
 413 track event. Clearly, the latter will always get the single-track events correct,
 414 and always get the multiple-track events wrong. We provide a comparison of
 415 these techniques in Table 2. As shown, the new algorithm classifies the number
 416 of muons in the detector 66% better than TTrigger.

417 5. Conclusions

418 We found that significant improvements can be achieved in the IceCube’s on-
 419 line track reconstruction by employing some classical data analysis algorithms.
 420 Optimizing data filtering and refining the least-square model have led to signif-
 421 icant improvements in the accuracy of the reconstruction direction. The new
 422 reconstruction software is fast enough to run on-site, and is now included in all
 423 IceCube analyses.

424 We also looked at the problem of determining the number of muons in the
 425 detector. We found that proximal clustering with some basic heuristics could
 426 correctly determine whether an event contained a single muon or multiple muons
 427 with less than 2% error, yielding an 66% improvement over the prior software.

428 References

- 429 [1] IceCube Collaboration, IceCube webpage, <http://icecube.wisc.edu/>.
- 430 [2] A. Achterberg et al., First year performance of the IceCube neutrino tele-
 431 scope, *Astroparticle Physics* 26 (3) (2006) 155–173.
- 432 [3] J.Ahrens et al., Muon track reconstruction and data selection techniques in
 433 AMANDA, *Nuclear Instruments and Methods in Physics Research Section*
 434 *A* 524 (2004) 169–194.
- 435 [4] M. G. Aartsen et al., Measurement of South Pole ice transparency with the
 436 IceCube LED calibration system IceCube Collaboration, *Nuclear Instru-*
 437 *ments and Methods in Physics Research Section A* (2013) 73–89.
- 438 [5] M. Ackermann et al., Optical properties of deep glacial ice at the south
 439 pole, *Journal of Geophysical Research* 111 (D13) (2006) D13203.

- 440 [6] F. Hirsch, on behalf of the ATLAS collaboration, Tracking and vertexing
441 with the ATLAS detector at the LHC, Nuclear Instruments and Methods
442 in Physics Research Section A: Accelerators, Spectrometers, Detectors and
443 Associated Equipment 650 (1) (2011) 218–223.
- 444 [7] R. S. Chivukulaa, M. Goldenaa, E. H. Simmons, Multi-jet physics at hadron
445 colliders, Nuclear Physics B 363 (1) (1991) 83–96.
- 446 [8] S. Ellis, J. Huston, K. Hatakeyama, P. Loch, M. Tönnesmann, Jets in
447 hadron–hadron collisions, Progress in Particle and Nuclear Physics (60)
448 (2008) 484–551.
- 449 [9] R. Abbasi et al., Calibration and characterization of the IceCube photomul-
450 tiplier tube, Nuclear Instruments and Methods in Physics Research Section
451 A 618 (2010) 139–152.
- 452 [10] R. Abbasi et al., The icecube data acquisition system: Signal capture, dig-
453 itization, and timestamping, Nuclear Instruments and Methods in Physics
454 Research Section A 601 (3) (2009) 294–316.
- 455 [11] M. Ackermann, Searches for signals from cosmic point-like sources of high
456 energy neutrinos in 5 years of AMANDA-II data, Ph.D. thesis, Humboldt-
457 Universität zu Berlin (2006).
- 458 [12] V. Stenger, Track fitting for DUMAND-II Octagon Array, Tech. rep., Uni-
459 versity of Hawaii at Manoa (1990).
- 460 [13] S. Boyd, L. Vandenberghe, Convex Optimization, Cambridge University
461 Press, 2009.
- 462 [14] R. Abbasi et al., Measurement of the atmospheric neutrino energy spectrum
463 from 100 GeV to 400 TeV with IceCube, Physical Review D 83 (1).
- 464 [15] D. Chirkin, Measurement of the atmospheric neutrino energy spectrum
465 with IceCube, Proceedings of the 31st ICRC.